

What Can Be Transferred: Unsupervised Domain Adaptation for Endoscopic Lesions Segmentation

Jiahua Dong^{1,2,3}, Yang Cong^{1,2*}, Gan Sun^{1,2*}, Bineng Zhong⁴ and Xiaowei Xu⁵

¹State Key Laboratory of Robotics, Shenyang Institute of Automation, Chinese Academy of Sciences, Shenyang, 110016, China.[†]

²Institutes for Robotics and Intelligent Manufacturing, Chinese Academy of Sciences, Shenyang, 110016, China.

³University of Chinese Academy of Sciences, Beijing, 100049, China.

⁴Huaqiao University, Xiamen, Fujian, 361021, China.

⁵Department of Information Science, University of Arkansas at Little Rock, Arkansas, USA.

dongjiahua@sia.cn, {congyang81, sungan1412}@gmail.com, bnzhong@hqu.edu.cn, xwxu@ualr.edu

Abstract

Unsupervised domain adaptation has attracted growing research attention on semantic segmentation. However, 1) most existing models cannot be directly applied into lesions transfer of medical images, due to the diverse appearances of same lesion among different datasets; 2) equal attention has been paid into all semantic representations instead of neglecting irrelevant knowledge, which leads to negative transfer of untransferable knowledge. To address these challenges, we develop a new unsupervised semantic transfer model including two complementary modules (i.e., \mathcal{T}_D and \mathcal{T}_F) for endoscopic lesions segmentation, which can alternatively determine where and how to explore transferable domain-invariant knowledge between labeled source lesions dataset (e.g., gastroscop) and unlabeled target diseases dataset (e.g., enteroscopy). Specifically, \mathcal{T}_D focuses on where to translate transferable visual information of medical lesions via residual transferability-aware bottleneck, while neglecting untransferable visual characterizations. Furthermore, \mathcal{T}_F highlights how to augment transferable semantic features of various lesions and automatically ignore untransferable representations, which explores domain-invariant knowledge and in return improves the performance of \mathcal{T}_D . To the end, theoretical analysis and extensive experiments on medical endoscopic dataset and several non-medical public datasets well demonstrate the superiority of our proposed model.

*The corresponding authors are Prof. Yang Cong and Dr. Gan Sun.

[†]This work is supported by Ministry of Science and Technology of the Peoples Republic of China (2019YFB1310300) and NSFC under grant (61722311, U1613214, 61821005, 61533015).

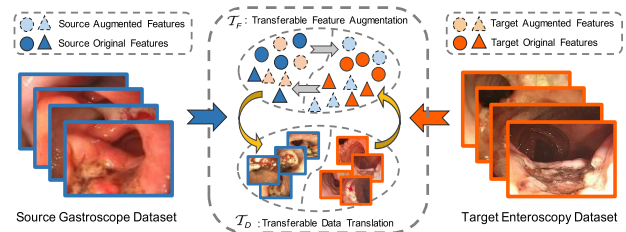


Figure 1. Illustration of our unsupervised semantic transfer model, where two complementary modules \mathcal{T}_F and \mathcal{T}_D can alternatively explore where to translate transferable visual characterizations of medical lesions and how to augment transferable semantic feature of various diseases, respectively.

1. Introduction

The successes of unsupervised domain adaptation have been widely-extended into a large amount of computer vision applications, e.g., semantic segmentation [16, 36]. Due to the powerful generalization capacity for segmentation task of unlabeled target data, enormous unsupervised domain adaptation methods [23, 25–27, 37] has been developed to narrow the distribution divergence between labeled source dataset and unlabeled target dataset.

However, most state-of-the-art models [8, 16, 17, 29] cannot efficiently address semantic transfer of medical lesions with various appearances, due to the difficulty in determining what kind of visual characterizations could boost or cripple the performance of semantic transfer. Additionally, they fail to brush untransferable representations aside while forcefully utilizing these irrelevant knowledge heavily degrades the transfer performance. *Take the clinical lesions diagnosis as an example, cancer and ulcer present diverse visual information (e.g., appearance, shape and tex-*

ture) among gastroscopy and enteroscopy datasets, which is a thorny diagnosis challenge due to the large distribution shift among different datasets. Obviously, it is difficult to manually determine what kind of lesions information could promote the transfer performance, i.e., exploring domain-invariant knowledge for various lesions. Therefore, how to automatically capture transferable visual characterizations and semantic representations while neglecting irrelevant knowledge across domains is our focus in this paper.

To address the above mentioned challenges, as shown in Figure 1, we develop a new unsupervised semantic lesions transfer model to mitigate the domain gap between labeled source lesions dataset (e.g., gastroscopy) and unlabeled target diseases dataset (e.g., enteroscopy). To be specific, the proposed model consists of two complementary modules, i.e., \mathcal{T}_D and \mathcal{T}_F , which could automatically determine where and how to explore transferable knowledge from source diseases dataset to assist target lesions segmentation task. On one hand, motivated by information theory [1], residual transferability-aware bottleneck is developed for \mathcal{T}_D to highlight where to translate transferable visual information while preventing irrelevant translation. On the other hand, Residual Attention on Attention Block (RA²B) is proposed to encode domain-invariant knowledge with high transferability scores, which assists \mathcal{T}_F in exploring how to augment transferable semantic features and boost the translation performance of module \mathcal{T}_D in return. Meanwhile, target samples are progressively assigned with confident pseudo pixel labels along the alternative training process of \mathcal{T}_D and \mathcal{T}_F , which further bridges the distribution shift in the retraining phase. Finally, theoretical analysis about our proposed model in term of narrowing domain discrepancy among source and target datasets is elaborated. Extensive experiments on both medical endoscopic dataset and several non-medical datasets are conducted to justify the effectiveness of our proposed model.

The main contributions of this paper are as follows:

- A new unsupervised semantic representations transfer model is proposed for endoscopic lesions segmentation. To our best knowledge, this is an earlier attempt to automatically highlight the transferable semantic knowledge for endoscopic lesions segmentation in the biomedical imaging field.
- Two complementary modules \mathcal{T}_D and \mathcal{T}_F are developed to alternatively explore the transferable representations while neglecting untransferable knowledge, which can not only determine where to translate transferable visual information via \mathcal{T}_D , but also highlight how to augment transferable representations via \mathcal{T}_F .
- Comprehensive theory analysis about how our model narrows domain discrepancy is provided. Experiments are also conducted to validate the superiority of our model against state-of-the-arts on the medical endo-

scopic dataset and several non-medical public datasets.

2. Related Work

This section reviews some related works about semantic lesions segmentation and unsupervised domain adaptation.

Semantic Segmentation of Lesions: Deep neural networks [39, 40] have achieved significant successes in enormous applications, e.g., medical lesions segmentation [3, 7, 16, 31, 42]. When compared with traditional models [12, 24] requiring handcrafted lesions features, it relies on powerful lesions characterization capacity to boost accuracy and efficiency of diseases diagnosis, but needs large-scale pixel labels. To save the annotations cost, unsupervised learning has been widely-applied into medical lesions segmentation [2, 4, 6, 7, 10, 17]. However, these models require effective prior information [10] or distribution hypothesis [2] to generalize previously unseen diseases, which only produces inaccurate and coarse lesions prediction. Thus, it is a thorny challenge to perform well on unseen target lesions when training on source diseases data [8, 16, 17].

Unsupervised Domain Adaptation: After Hoffman *et al.* [22] first utilize adversarial network [19] to achieve domain adaptation for semantic segmentation task, diverse variants based on adversarial strategy [11, 23, 34, 35, 37, 41] are proposed to address the domain shift challenge. Different from these models, [27, 43] employ curriculum learning to infer important properties for target images according to source samples. [45] designs a non-adversarial model to transfer semantic representation in a self-training manner. [18] presents the domain flow translation to explore expected intermediate domain. Li *et al.* [26] propose a bidirectional learning model for target adaptation. In addition, novel adaptation losses [25, 29, 38] are designed to measure discrepancy among different datasets. [16] develop a pseudo pixel label generator to focus on hard-to-transfer target samples. [14, 15, 28, 30, 36] explore discriminative semantic knowledge to narrow the distribution divergence.

3. The Proposed Model

In this section, we first present overall framework of our proposed model and then introduce detailed model formulation, followed by comprehensive theoretical analysis.

3.1. Overview

Given the source dataset (e.g., gastroscopy) $X_s = \{x_i^s, y_i^s\}_{i=1}^m$ and target dataset (e.g., enteroscopy) $X_t = \{x_j^t\}_{j=1}^n$, where x_i^s and x_j^t represent source samples with pixel annotations y_i^s and target images without pixel labels, respectively. Although existing semantic transfer models [25, 28, 29, 36, 38] attempt to narrow the distribution shift among source and target datasets, semantic representations are not all transferable while forcefully taking advantage of

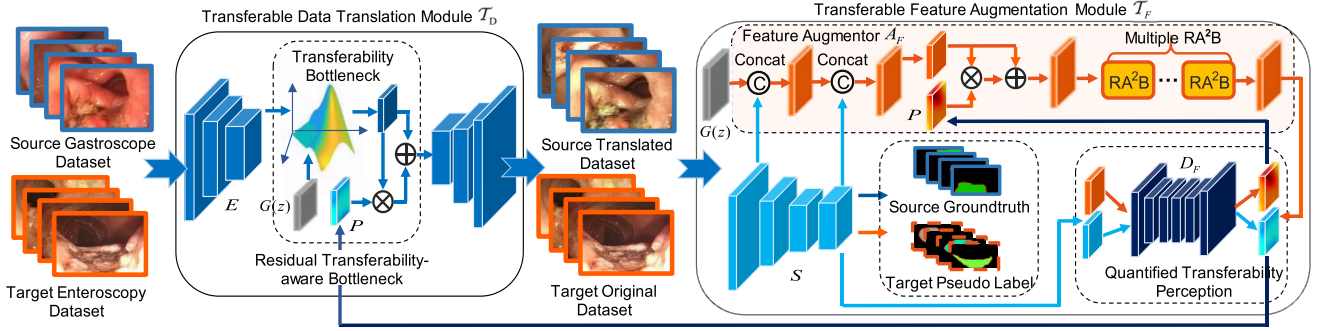


Figure 2. Overview architecture of our proposed model, which is composed of two alternatively complementary modules \mathcal{T}_D and \mathcal{T}_F . Specifically, \mathcal{T}_D focuses on exploring where to translate transferable visual characterizations via residual transferability-aware bottleneck. \mathcal{T}_F highlights how to augment transferable semantic representations while neglecting untransferable knowledge, which incorporates multiple residual attention on attention blocks (RA²B) to capture domain-invariant features with high transferability.

irrelevant knowledge could lead to negative transfer. Besides, various lesions with diverse appearances make them difficult to explore what kind of visual characterizations will promote transfer performance. Therefore, we endeavor to automatically highlight the transferable representations between source and target datasets to improve the lesions segmentation performance for unlabeled target samples, while ignoring the irrelevant knowledge for semantic transfer.

As depicted in Figure 2, the proposed model consists of two complementary modules, *i.e.*, \mathcal{T}_D and \mathcal{T}_F , which alternatively determines where and how to highlight transferable knowledge. Specifically, with quantified transferability perception from discriminator D_F in \mathcal{T}_F , the source samples x_i^s are first passed into \mathcal{T}_D to explore where to translate transferable visual characterizations, according to the style information of target images x_j^t . Afterwards, we forward the translated source samples \hat{x}_i^s along with x_j^t into \mathcal{T}_F to determine how to augment transferable semantic features while ignoring those untransferable representations. \mathcal{T}_F further mitigates the domain gap in the feature space and in return promotes the translation performance of \mathcal{T}_D . Our model could be regarded as a closed loop to alternatively update the parameters of \mathcal{T}_D and \mathcal{T}_F . Furthermore, along the alternative training process of \mathcal{T}_D and \mathcal{T}_F , our model progressively mines confident pseudo pixel labels \hat{y}_j^t for target samples, which fine-tunes the segmentation model S in \mathcal{T}_F to learn domain-invariant knowledge.

3.2. Quantified Transferability Perception

Intuitively, domain uncertainty estimation of the discriminator D_F in \mathcal{T}_F can assist in identifying those representations which can be transferred, cannot be transferred, or already transferred. For example, the input source features F_s and target features F_t that are already aligned across domains will fool the discriminator D_F for distinguishing whether the input is from X_s or X_t . In other words, we can easily discriminate whether the input feature maps F_s or F_t is transferable or not according to the output

probabilities of discriminator D_F . Therefore, in order to highlight those transferable representations, we utilize uncertainty measure function of information theory (*i.e.*, entropy criterion $\mathcal{I}(p) = -\sum_r p_r \log(p_r)$) to quantify the transferability perception of corresponding semantic features. Take the source samples as an example, given the output probability $D_F(F_s; \theta_{D_F})$ of discriminator D_F with network weights θ_{D_F} , the transferability perception for input source feature F_s can be formally quantified as follows:

$$P = 1 - \mathcal{I}(D_F(F_s; \theta_{D_F})). \quad (1)$$

Similarly, Eq. (1) can also quantify the transferability for target features F_t according to the output $D_F(F_t; \theta_{D_F})$. Note that the quantified transferability for source and target features share the same notation P for simplification.

However, false transferability perception may hurt semantic transfer task to some degree. Therefore, residual transferability perception mechanism is designed to feedback the positive transferability into \mathcal{T}_D in Section 3.3 and feature augmentor A_F in Section 3.4, as shown in Figure 2.

3.3. Transferable Data Translation (\mathcal{T}_D)

Different from previous translation model [21], our module \mathcal{T}_D could highlight where to translate transferable visual characterizations for better transfer performance. With the quantified transferability perception from D_F , \mathcal{T}_D pays more attention to selectively explore transferable mappings $X_s \rightarrow X_t$ and $X_t \rightarrow X_s$ while preventing irrelevant translations with low transfer scores. The samples from both X_s and X_t are forwarded into \mathcal{T}_D to train the translation model, which produces the corresponding translated source dataset $\hat{X}_s = \{\hat{x}_i^s, y_i^s\}_{i=1}^m$ and mapped target dataset $\hat{X}_t = \{\hat{x}_j^t\}_{j=1}^n$. $\hat{x}_i^s = \mathcal{T}_D(x_i^s; \theta_{\mathcal{T}_D})$ and $\hat{x}_j^t = \mathcal{T}_D^{-1}(x_j^t; \theta_{\mathcal{T}_D^{-1}})$ correspond to translated samples from \hat{X}_s and \hat{X}_t , where $\theta_{\mathcal{T}_D}$ and $\theta_{\mathcal{T}_D^{-1}}$ are network parameters of \mathcal{T}_D and \mathcal{T}_D^{-1} , respectively, and \mathcal{T}_D^{-1} denotes the reverse translation of \mathcal{T}_D that learns the mapping $X_t \rightarrow X_s$. Notice that translated source

images \hat{x}_i^s share same pixel annotations y_i^s with original image x_i^s , though there exists large visual gap among them. To encourage \hat{X}_s have closer distribution with X_t , $\mathcal{L}_d^a(\hat{X}_s, X_t)$ is employed to train \mathcal{T}_D , which can be written as follows:

$$\begin{aligned} \mathcal{L}_d^a(\hat{X}_s, X_t) = & \mathbb{E}_{x_j^t \in X_t} [\log(D_1(x_j^t; \theta_{D_1}))] + \\ & \mathbb{E}_{x_i^s \in X_s} [1 - \log(D_1(\mathcal{T}_D(x_i^s; \theta_{\mathcal{T}_D}); \theta_{D_1}))], \end{aligned} \quad (2)$$

where D_1 is the discriminator with network parameters θ_{D_1} that distinguishes between translated source images \hat{x}_i^s and real target samples x_j^t . Likewise, we utilize $\mathcal{L}_d^a(X_s, \hat{X}_t)$ to learn the mapping translation from X_t to X_s , *i.e.*,

$$\begin{aligned} \mathcal{L}_d^a(X_s, \hat{X}_t) = & \mathbb{E}_{x_i^s \in X_s} [\log(D_2(x_i^s; \theta_{D_2}))] + \\ & \mathbb{E}_{x_j^t \in X_t} [1 - \log(D_2(\mathcal{T}_D^{-1}(x_j^t; \theta_{\mathcal{T}_D^{-1}}); \theta_{D_2}))], \end{aligned} \quad (3)$$

where D_2 shares similar definition with D_1 but discriminates whether the inputs are from real source images x_i^s or translated target samples \hat{x}_j^t . θ_{D_2} represents the corresponding network weights of D_2 . Additionally, semantic consistency between input and reconstructed samples for both source and target data are ensured by the loss $\mathcal{L}_d^c(X_s, X_t)$:

$$\begin{aligned} \mathcal{L}_d^c(X_s, X_t) = & \mathbb{E}_{x_j^t \in X_t} [\|\mathcal{T}_D(\hat{x}_j^t; \theta_{\mathcal{T}_D}) - x_j^t\|_1] + \\ & \mathbb{E}_{x_i^s \in X_s} [\|\mathcal{T}_D^{-1}(\hat{x}_i^s; \theta_{\mathcal{T}_D^{-1}}) - x_i^s\|_1]. \end{aligned} \quad (4)$$

As a result, the overall objective $\mathcal{L}_{\mathcal{T}_D}$ for training \mathcal{T}_D is:

$$\mathcal{L}_{\mathcal{T}_D} = \mathcal{L}_d^a(\hat{X}_s, X_t) + \mathcal{L}_d^a(X_s, \hat{X}_t) + \alpha \mathcal{L}_d^c(X_s, X_t). \quad (5)$$

However, Eq. (5) cannot selectively capture important semantic knowledge with high transferability. Therefore, as shown in Figure 2, we develop a residual transferability-aware bottleneck, which determines where to translate transferable information by purifying semantic knowledge with high transfer scores. Specifically, built upon the information theory [1], we design an information constraint on the latent feature space, which is adaptively weighted by the quantified transferability perception P in Eq. (1). It encourages the feature extractor E in \mathcal{T}_D to encode transferable representations. Formally, Eq. (5) can be reformulated as:

$$\begin{aligned} \mathcal{L}_{\mathcal{T}_D} = & \mathcal{L}_d^a(\hat{X}_s, X_t) + \mathcal{L}_d^a(X_s, \hat{X}_t) + \alpha \mathcal{L}_d^c(X_s, X_t), \\ \text{s.t. } & \mathbb{E}_{x_i^s \in X_s} [P \odot \text{KL}(E(x_i^s; \theta_E) \| G(z))] \leq T_s, \\ & \mathbb{E}_{x_j^t \in X_t} [P \odot \text{KL}(E(x_j^t; \theta_E) \| G(z))] \leq T_t, \end{aligned} \quad (6)$$

where \odot represents the channel-wise product. $G(z)$ is the marginal distribution of z , which denotes the standard Gaussian distribution $\mathcal{N}(0; I)$. T_s and T_t represent transferability bottleneck thresholds for source and target datasets, respectively. They are set as the same value in this paper and denoted as T for simplification. $E(x_i^s; \theta_E)$ and $E(x_j^t; \theta_E)$

are the extracted features via E for source and target samples, where θ_E denotes the network parameters. Take samples x_i^s as the intuitive explanation for Eq. (6): the larger KL divergence among $E(x_i^s; \theta_E)$ and $G(z)$ indicates the closer dependence among x_i^s and z , which enforces z to encode more semantic representations from samples x_i^s . Obviously, these semantic representations are not all transferable for translation while utilizing irrelevant knowledge leads to the negative transfer. Thus, by enforcing KL divergence weighted with quantified transferability P to the threshold T , untransferable representations from $G(z)$ could be neglected, which is then regarded as latent feature of x_i^s and forwarded into the decoder network. To optimize Eq. (6), we equally formulate it as Eq. (7) by employing two Lagrange multipliers λ_s and λ_t for source and target datasets:

$$\begin{aligned} \mathcal{L}_{\mathcal{T}_D} = & \mathcal{L}_d^a(\hat{X}_s, X_t) + \mathcal{L}_d^a(X_s, \hat{X}_t) + \alpha \mathcal{L}_d^c(X_s, X_t) \\ & + \lambda_s (\mathbb{E}_{x_i^s \in X_s} [P \odot (\text{KL}(E(x_i^s; \theta_E) \| G(z)) - T)]) \\ & + \lambda_t (\mathbb{E}_{x_j^t \in X_t} [P \odot (\text{KL}(E(x_j^t; \theta_E) \| G(z)) - T)]), \end{aligned} \quad (7)$$

where λ_s and λ_t are updated by $\lambda_s \leftarrow \max(\lambda_s, \gamma \mathcal{L}_b^s)$ and $\lambda_t \leftarrow \max(\lambda_t, \gamma \mathcal{L}_b^t)$, respectively. The last two terms of Eq. (7) are defined as the transferability constraint losses \mathcal{L}_b^s and \mathcal{L}_b^t . γ denotes the updating step of λ_s and λ_t .

3.4. Transferable Feature Augmentation (\mathcal{T}_F)

Although \mathcal{T}_D is designed to translate transferable visual characterizations, it cannot ensure feature distribution across domains to be well aligned. Motivated by this observation, transferable feature augmentation module \mathcal{T}_F is developed to automatically determine how to augment transferable semantic features, which further mitigates the domain gap among different datasets and in return boosts the performance of \mathcal{T}_D . As depicted in Figure 2, feature augmentor A_F encodes transferable representations from low-level and high-level layers that preserve informative details by incorporating with multiple residual attention on attention blocks (RA²B), where RA²B focuses on highlighting the relevance transferability of transferable representations and the details of RA²B are presented as follows.

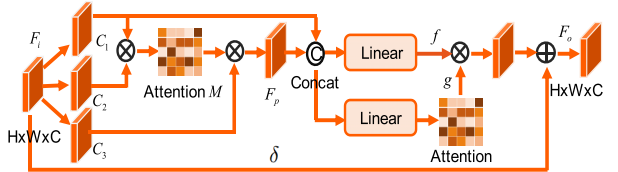


Figure 3. The detailed illustration of RA²B.

As shown in Figure 3, given the input feature $F_i \in \mathbb{R}^{H \times W \times C}$, we forward it into three convolutional blocks to produce three new features C_1, C_2 and C_3 ($C_1, C_2, C_3 \in \mathbb{R}^{H \times W \times C}$), where H, W and C represent the height, width and channels of corresponding features. After reshaping

C_1 and C_2 into $\mathbb{R}^{N \times C}$ ($N = H \times W$ denotes the number of pixel positions), attention matrix $M = \{M_{ij}\}_{i,j=1}^N \in \mathbb{R}^{N \times N}$ with softmax activation is obtained. We then utilize the matrix multiplication operator between the transpose of M and reshaped $C_3 \in \mathbb{R}^{N \times C}$ to output the attention feature map $F_p \in \mathbb{R}^{N \times C}$, where M and F_p can be formulated as:

$$M_{ij} = \frac{\exp((C_1 C_2^\top)_{ij})}{\sum_{i=1}^N \exp((C_1 C_2^\top)_{ij})}, (F_p)_i = \sum_{j=1}^N M_{ij} (C_3)_j, \quad (8)$$

where $(F_p)_i$ and $(C_3)_j$ respectively denote the corresponding features at the i -th and j -th pixel positions. Even though there is no relevant transferable features, Eq. (8) still generates an average weighted feature map F_p , which could heavily degrade the transferability of semantic knowledge or even encourage them to be untransferable.

Therefore, we develop the RA²B module to measure the relevance between attention result F_p and input feature C_1 . Then the transferable information flow f and relevance gate g are produced via the linear operation on F_p and C_1 , *i.e.*,

$$\begin{aligned} f &= W_f^1 C_1 + W_f^2 F_p + B_f, \\ g &= \text{sigmoid}(W_g^1 C_1 + W_g^2 F_p + B_g), \end{aligned} \quad (9)$$

where $W_f^1, W_f^2, W_g^1, W_g^2 \in \mathbb{R}^{N \times N}$, $B_f, B_g \in \mathbb{R}^{N \times C}$ are the transformation matrices. Afterwards, f and g are reshaped into $\mathbb{R}^{H \times W \times C}$ and employed to perform element-wise multiplication. We multiply the produced result by a scalar parameter δ and employ an element-wise sum operation with F_i to obtain the ultimate feature $F_o \in \mathbb{R}^{H \times W \times C}$:

$$F_o = \delta(f \otimes g) + F_i, \quad (10)$$

where δ is initialized as 0, and its value is adaptively learned along the training process.

With quantified transferability perception from D_F , A_F could selectively augment the transferable representations while preventing the irrelevant augmentation, which promotes the segmentation module S to learn domain-invariant knowledge and further improves the performance of \mathcal{T}_D in return. The details about how to train \mathcal{T}_F are as follows:

Step I: The translated source samples \hat{x}_i^s with pixel annotations y_i^s and target images x_j^t with generated pseudo pixel labels \hat{y}_j^t are forwarded into segmentation model S , where $\hat{y}_j^t = \text{argmax}(S(x_j^t; \theta_S))$ and θ_S indicates network weights of S . The segmentation loss \mathcal{L}_f^s for training S can be concretely expressed as:

$$\begin{aligned} \min_{\theta_S} \mathcal{L}_f^s &= \mathbb{E}_{(\hat{x}_i^s, y_i^s) \in \hat{X}_s} \left[- \sum_{u=1}^{|\hat{x}_i^s|} \sum_{k=1}^K \mathbf{1}_{k=(y_i^s)_u} \log(S(\hat{x}_i^s; \theta_S)_u^k) \right] \\ &+ \mathbb{E}_{(x_j^t, \hat{y}_j^t) \in X_t} \left[- \sum_{v=1}^{|\hat{x}_j^t|} M_v \sum_{k=1}^K \mathbf{1}_{k=(\hat{y}_j^t)_v} \log(S(x_j^t; \theta_S)_v^k) \right], \end{aligned} \quad (11)$$

where $S(\hat{x}_i^s; \theta_S)_u^k$ and $S(x_j^t; \theta_S)_v^k$ denote the output probabilities of S predicted as class k at the u -th and the v -th pixels, respectively. K is the classes number. $M_v = \mathbf{1}_{\max(S(x_j^t; \theta_S)_v) \geq \beta}$ generates confident pseudo labels at v -th pixel for training, where $\beta = 0.9$ is a probability threshold.

Step II: In order to encourage A_F synthesize new transferable features that resemble the extracted features from source or target datasets (*i.e.*, feature augmentation), D_F is employed to distinguish whether the input is from A_F or S . Intuitively, with the assistance of quantified transferability P from D_F , A_F selectively augments transferable domain-invariant features while neglecting untransferable knowledge. Consequently, \mathcal{L}_f^a is designed to train A_F while fixing the parameters of S learned from **Step I**:

$$\begin{aligned} \min_{\theta_{A_F}} \max_{\theta_{D_F}} \mathcal{L}_f^a &= \mathbb{E}_{x \in (\hat{X}_s, X_t)} [\log(D_F(S(x; \theta_S); \theta_{D_F}))] + \\ &\mathbb{E}_{x \in (\hat{X}_s, X_t), z \in G(z)} [\log(1 - D_F(A_F(x, z; \theta_{A_F}); \theta_{D_F}))], \end{aligned} \quad (12)$$

where θ_{A_F} are parameters of A_F . $G(z) = \mathcal{N}(0; I)$ denotes Gaussian distribution from which noise samples are drawn.

Step III: The network weights of A_F learned in **Step II** are fixed in **Step III**. D_F is retrained to discriminate whether the input is from original datasets or augmented transferable representation. It encourages S to explore a common feature space, where target features are indistinguishable from the source one. As a result, the training objective \mathcal{L}_f^t in Eq. (13) is proposed to optimize S , which captures transferable domain invariant knowledge while neglecting the untransferable representations.

$$\begin{aligned} \min_{\theta_S} \max_{\theta_{D_F}} \mathcal{L}_f^t &= \mathbb{E}_{x \in (\hat{X}_s, X_t)} [\log(1 - D_F(S(x; \theta_S); \theta_{D_F}))] \\ &+ \mathbb{E}_{x \in (\hat{X}_s, X_t), z \in G(z)} [\log(D_F(A_F(x, z; \theta_{A_F}); \theta_{D_F}))], \end{aligned} \quad (13)$$

Notice that the quantified transferability perception P in Section 3.2 is from D_F in **Step III** rather than **Step II**.

3.5. Implementation Details

Network Architecture: For the transferable visual translation module \mathcal{T}_D , CycleGAN [44] is employed as the baseline network. As depicted in Figure 2, the residual transferability-aware bottleneck is attached on the last convolutional block of \mathcal{T}_D . In the transferable feature augmentation module \mathcal{T}_F , segmentation network S is DeepLabv3 [9] with ResNet-101 [20] as the backbone architecture, whose the strides of the last two convolutional blocks are transformed from 2 to 1 for higher dimension output. A_F encodes the features from the bottom and the last convolutional blocks of S , which are first augmented with the noise from Gaussian distribution. For discriminator D_F , we utilize 5 fully convolutional layers with channel number as

Table 1. Performance comparison between our proposed model and several competing methods on medical endoscopic dataset.

Metrics	BL [9]	LtA [37]	CGAN [23]	CLAN [29]	ADV [38]	BDL [26]	SWES [16]	DPR [36]	PyCDA [27]	Ours
IoU _n (%)	74.47	81.04	79.75	81.74	81.95	84.22	83.96	83.23	84.31	85.48
IoU _d (%)	32.65	40.35	40.52	41.33	42.27	42.84	42.63	42.11	43.08	43.67
mIoU(%)	53.56	60.70	60.13	61.54	62.11	63.53	63.29	62.67	63.70	64.58

{16, 32, 64, 64, 1}, where the leaky RELU function parameterized by 0.2 is employed to activate each layer excluding the last convolution filter activated by the sigmoid function.

Training and Testing: Two complementary modules \mathcal{T}_D and \mathcal{T}_F are alternatively trained until convergence. When training the network \mathcal{T}_D , inspired by [44], we set $\alpha = 10$. The learning rate is initialized as 2.5×10^{-4} for first 10 epochs and linearly decreases to 0 in the later 5 epochs. In Eq. (7), $T = 200$, λ_s and λ_t are initialized as 1.0×10^{-4} with updating step γ as 1.0×10^{-6} . For backbone DeepLab-v3 [9], we utilize SGD optimizer with an initial learning rate as 2.0×10^{-4} and power as 0.9. The Adam optimizer with initial learning rate as 1.0×10^{-4} is employed for training D_F . We set its momentum as 0.9 and 0.99. In the testing stage, the target images x_j^t (e.g., enteroscopy) are directly forwarded into S for evaluation.

3.6. Theoretical Analysis

In this subsection, we elaborate the theoretical analysis about our model in term of narrowing domain discrepancy $d_{\mathcal{H}}(P_s, P_t)$ between source and target distributions (P_s and P_t), with regard to the hypothesis set \mathcal{H} . As pointed out by [5], the expected error $\epsilon^{P_t}(h)$ of any classifier $h \in \mathcal{H}$ performing on target dataset has theory upper bound, i.e.,

$$\forall h \in \mathcal{H}, \epsilon^{P_t}(h) \leq \epsilon^{P_s}(h) + \frac{1}{2}d_{\mathcal{H}}(P_s, P_t) + \Gamma, \quad (14)$$

where Γ is an independent constant. $\epsilon^{P_s}(h)$ is the expected error of any $h \in \mathcal{H}$ classifying on source samples, which can be negligibly small under the supervisory training. $d_{\mathcal{H}}(P_s, P_t) = 2 \sup_{h \in \mathcal{H}} |\Pr_{x_i^s \sim P_s}[h(x_i^s) = 1] - \Pr_{x_j^t \sim P_t}[h(x_j^t) = 1]|$ denotes the \mathcal{H} -divergence distance between P_s and P_t . Thus, the relationships between our model and domain discrepancy $d_{\mathcal{H}}(P_s, P_t)$ will be discussed.

As the metric distance of distributions P_s and P_t , $d_{\mathcal{H}}(P_s, P_t)$ satisfies the following triangle inequality, i.e.,

$$d_{\mathcal{H}}(P_s, P_t) \leq d_{\mathcal{H}}(P_s, G(z)) + d_{\mathcal{H}}(P_t, G(z)), \quad (15)$$

where $G(z) = \mathcal{N}(0; I)$ is the marginal distribution of z .

Recall that two complementary modules \mathcal{T}_D and \mathcal{T}_F (Eq. (7) and Eq. (13)) alternatively prevent the negative transfer of untransferable knowledge, which encourages the distributions of both P_s and P_t tend to the standard Gaussian, i.e., $P_s \rightarrow \mathcal{N}(0; I)$ and $P_t \rightarrow \mathcal{N}(0; I)$. Consequently, our proposed model forces the last two terms of

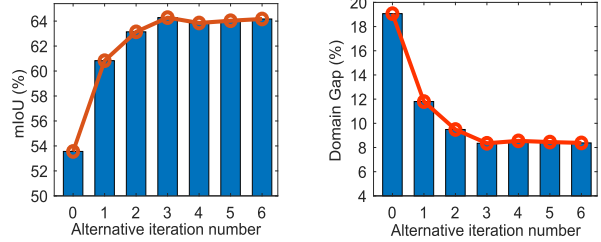


Figure 4. The complementary effect of modules \mathcal{T}_D and \mathcal{T}_F about mIoU (left) and domain gap (right) on the endoscopic dataset.

Eq. (15) to be near zero, i.e., $d_{\mathcal{H}}(P_s, G(z)) \rightarrow 0$ and $d_{\mathcal{H}}(P_t, G(z)) \rightarrow 0$. In summary, our model could efficiently achieve the tighter upper bound for target excepted error $\epsilon^{P_t}(h)$ and reduce domain discrepancy $d_{\mathcal{H}}(P_s, P_t)$.

4. Experiments

4.1. Datasets and Evaluation

Medical Endoscopic Dataset [16] is collected from various endoscopic lesions, i.e., cancer, polyp, gastritis, ulcer and bleeding. Specifically, it consists of 2969 gastroscoposcope samples and 690 enteroscopy images. For the training phase, 2969 gastroscoposcope images with pixel annotations are regarded as the source data. We treat 300 enteroscopy samples without pixel labels as target data. In the testing stage, we use the other 390 enteroscopy samples for evaluation.

Cityscapes [13] is a real-world dataset about European urban street scenes, which is collected from 50 cities and has total 34 defined categories. It is composed of three disjoint subsets with 2993, 503 and 1531 images for training, testing and validation, respectively.

GTA [32] consists of 24996 images generated from fictional city scenes of Los Santos in the computer game Grand Theft Auto V. The annotation categories are compatible with the Cityscapes dataset [13].

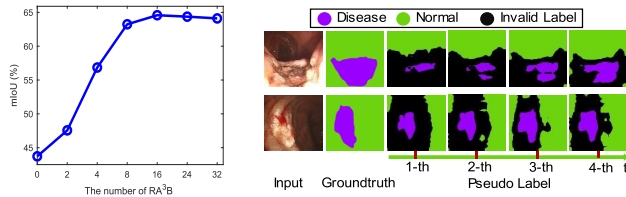
SYNTIA [33] is a large-scale synthetic dataset whose urban scenes are collected from virtual city without corresponding to any realistic city. We utilize its subset called SYNTIA-RANDCITYSCAPES in our experiments, which contains 9400 images with 12 automatically labeled object classes and some undefined categories.

Evaluation Metric: Intersection over union (IoU) is regarded as basic evaluation metric. Besides, we utilize three derived metrics, i.e., mean IoU (mIoU), IoU of normal (IoU_n), and IoU of disease (IoU_d).

Notations: In all experiments, BL represents the baseline network DeepLab-v3 [9] without semantic transfer.

Table 2. Ablation experiments on the medical endoscopic datasets.

Variants	QT	PL	TKB	AA	mIoU(%)	Δ (%)
Ours-w/oQT		✓	✓	✓	61.47	-3.11
Ours-w/oPL	✓		✓	✓	61.35	-3.23
Ours-w/oTKB	✓	✓		✓	62.73	-1.85
Ours-w/oAA	✓	✓	✓		63.06	-1.52
Ours	✓	✓	✓	✓	64.58	-



(a) Number of RA²B (b) Pseudo labels

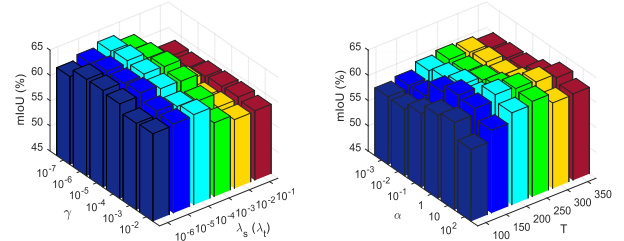
Figure 5. The effect of different number of RA²B (left), and the generation process of pseudo labels along the alternative iteration number of modules \mathcal{T}_D and \mathcal{T}_F (right) on the medical dataset.

4.2. Experiments on Medical Endoscopic Dataset

In our experiments, all the competing methods in Table 1 employ ResNet-101 [20] as backbone architecture for a fair comparison. From the presented results in Table 1, we can observe that: 1) Our model could significantly mitigate the domain gap about 11.02% between source and target datasets when comparing with baseline BL [9]. 2) Existing transfer models [16, 26, 27, 36, 38] perform worse than our model, since they pay equal attention to all semantic representation instead of neglecting irrelevant knowledge, which causes the negative transfer of untransferable knowledge.

Effect of Complementary Modules \mathcal{T}_D and \mathcal{T}_F : This subsection introduces alternative iteration experiments to validate the effectiveness of complementary modules \mathcal{T}_D and \mathcal{T}_F . As shown in Figure 4, \mathcal{T}_D and \mathcal{T}_F can mutually promote each other and progressively narrow the domain gap along the alternative iteration process. After a few iterations (e.g., the number is 3 for this medical dataset), the performance of our model achieves efficient convergence. After using \mathcal{T}_D to translate transferable visual information, \mathcal{T}_F can further automatically determine how to augment transferable semantic features and in return promote the translation performance of \mathcal{T}_D . The experimental results are in accordance with the theoretical analysis in Section 3.6.

Ablation Studies: To verify the importance of different components in our proposed model, we intend to conduct the variant experiments with the ablation of different components on medical endoscopic dataset, i.e., quantified transferability (QT), pseudo labels (PL), transferability-aware bottleneck (TKB) and attention on attention (AA) of RA²B. Training the model without QT, PL, TKB and AA are respectively denoted as Ours-w/oQT, Ours-w/oPL, Ours-w/oTKB and Ours-w/oAA. From the presented results in Table 2, we can notice that the performance de-



(a) $\alpha = 10, T = 200$ (b) $\gamma = 10^{-6}, \lambda_s(\lambda_t) = 10^{-4}$

Figure 6. The parameters investigations about $\{\gamma, \lambda_s(\lambda_t)\}$ (left) and $\{\alpha, T\}$ (right) on the medical dataset.

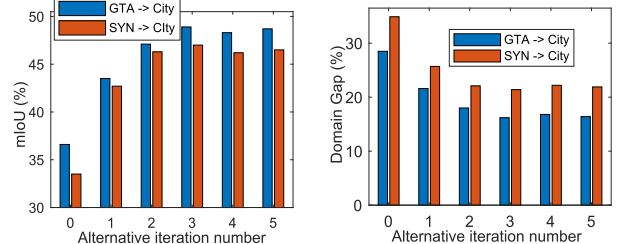


Figure 7. The complementary effect of modules \mathcal{T}_D and \mathcal{T}_F about mIoU (left) and domain gap (right) on several benchmark datasets.

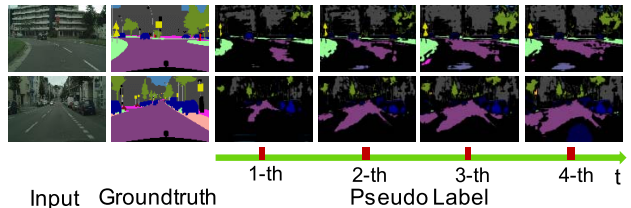


Figure 8. Pseudo Labels generated along the alternative iteration number of modules \mathcal{T}_D and \mathcal{T}_F on GTA \rightarrow Cityscapes task.

grades 1.52% \sim 3.23% after removing any component of our model, which justifies the rationality and effectiveness of each designed component. Besides, with quantified transferability perception from D_F , our model could efficiently encode transferable semantic knowledge among source and target datasets while brushing irrelevant representations aside. Multiple RA²Bs play an essential role in capturing the relevance transferability of transferable knowledge and we set its number as 16, as illustrated in Figure 5 (a). Moreover, the distribution shift between different datasets could be further bridged by confident pseudo labels, which are generated progressively along the iteration process, as depicted in Figure 5 (b).

Parameters Investigations: In this subsection, extensive hyper-parameter experiments are empirically conducted to investigate the effect of hyper-parameters $\{\alpha, T\}$ and $\{\gamma, \lambda_s(\lambda_t)\}$, which assists to determine the optimal parameters. λ_s and λ_t share same value in our experiments. Notice that our model achieves stable performance over the wide range of different parameters, as shown in Figure 6. Furthermore, it also validates that residual transferability-aware bottleneck in Eq. (7) can efficiently purify the transferable semantic representations with high transfer scores.

Table 3. Performance comparison of transferring semantic representations from GTA to Cityscapes.

Method	road	sidewalk	building	wall	fence	pole	light	sign	veg	terrain	sky	person	rider	car	truck	bus	train	mbike	bike	mIoU(%)
LtA [37]	86.5	36.0	79.9	23.4	23.3	23.9	35.2	14.8	83.4	33.3	75.6	58.5	27.6	73.7	32.5	35.4	3.9	30.1	28.1	42.4
MCD [34]	90.3	31.0	78.5	19.7	17.3	28.6	30.9	16.1	83.7	30.0	69.1	58.5	19.6	81.5	23.8	30.0	5.7	25.7	14.3	39.7
CGAN [23]	89.2	49.0	70.7	13.5	10.9	38.5	29.4	33.7	77.9	37.6	65.8	75.1	32.4	77.8	39.2	45.2	0.0	25.2	35.4	44.5
CBST [45]	88.0	56.2	77.0	27.4	22.4	40.7	47.3	40.9	82.4	21.6	60.3	50.2	20.4	83.8	35.0	51.0	15.2	20.6	37.0	46.2
CLAN [29]	87.0	27.1	79.6	27.3	23.3	28.3	35.5	24.2	83.6	27.4	74.2	58.6	28.0	76.2	33.1	36.7	6.7	31.9	31.4	43.2
SWD [25]	92.0	46.4	82.4	24.8	24.0	35.1	33.4	34.2	83.6	30.4	80.9	56.9	21.9	82.0	24.4	28.7	6.1	25.0	33.6	44.5
ADV [38]	89.4	33.1	81.0	26.6	26.8	27.2	33.5	24.7	83.9	36.7	78.8	58.7	30.5	84.8	38.5	44.5	1.7	31.6	32.5	45.5
BDL [26]	91.0	44.7	84.2	34.6	27.6	30.2	36.0	36.0	85.0	43.6	83.0	58.6	31.6	83.3	35.3	49.7	3.3	28.8	35.6	48.5
SWLS [16]	92.7	48.0	78.8	25.7	27.2	36.0	42.2	45.3	80.6	14.6	66.0	62.1	30.4	86.2	28.0	45.6	35.9	16.8	34.7	47.2
DPR [36]	92.3	51.9	82.1	29.2	25.1	24.5	33.8	33.0	82.4	32.8	82.2	58.6	27.2	84.3	33.4	46.3	2.2	29.5	32.3	46.5
PyCDA [27]	90.5	36.3	84.4	32.4	28.7	34.6	36.4	31.5	86.8	37.9	78.5	62.3	21.5	85.6	27.9	34.8	18.0	22.9	49.3	47.4
BL	75.8	16.8	77.2	12.5	21.0	25.5	30.1	20.1	81.3	24.6	70.3	53.8	26.4	49.9	17.2	25.9	6.5	25.3	36.0	36.6
Ours-w/oQT	89.0	40.0	83.4	34.0	23.7	32.2	36.6	33.1	84.0	39.3	74.3	58.9	27.2	78.8	32.6	35.1	0.1	28.4	37.4	45.7
Ours-w/oPL	90.6	40.8	84.1	31.3	22.7	32.0	39.0	33.7	84.3	39.5	80.7	58.4	28.7	82.8	27.4	48.1	1.0	27.0	28.5	46.4
Ours-w/oTKB	88.9	45.2	82.9	32.7	26.6	31.5	34.8	34.3	83.5	38.8	81.5	60.0	31.5	80.6	30.8	44.9	5.2	33.8	35.4	47.5
Ours-w/oAA	89.1	49.8	82.7	32.8	26.6	32.0	35.8	32.4	83.1	37.2	83.8	58.7	32.9	81.0	34.9	47.1	1.5	33.1	36.8	48.0
Ours	89.4	50.1	83.9	35.9	27.0	32.4	38.6	37.5	84.5	39.6	85.7	61.6	33.7	82.2	36.0	50.4	0.3	33.6	32.1	49.2

Table 4. Performance comparison of transferring semantic knowledge from SYNTHIA to Cityscapes.

Method	road	sidewalk	building	wall	fence	pole	light	sign	veg	sky	person	rider	car	bus	mbike	bike	mIoU(%)
LSD [35]	80.1	29.1	77.5	2.8	0.4	26.8	11.1	18.0	78.1	76.7	48.2	15.2	70.5	17.4	8.7	16.7	36.1
MCD [34]	84.8	43.6	79.0	3.9	0.2	29.1	7.2	5.5	83.8	83.1	51.0	11.7	79.9	27.2	6.2	0.0	37.3
CGAN [23]	85.0	25.8	73.5	3.4	3.0	31.5	19.5	21.3	67.4	69.4	68.5	25.0	76.5	41.6	17.9	29.5	41.2
DCAN [41]	82.8	36.4	75.7	5.1	0.1	25.8	8.0	18.7	74.7	76.9	51.1	15.9	77.7	24.8	4.1	37.3	38.4
CBST [45]	53.6	23.7	75.0	12.5	0.3	36.4	23.5	26.3	84.8	74.7	67.2	17.5	84.5	28.4	15.2	55.8	42.5
ADV [38]	85.6	42.2	79.7	8.7	0.4	25.9	5.4	8.1	80.4	84.1	57.9	23.8	73.3	36.4	14.2	33.0	41.2
SWLS [16]	68.4	30.1	74.2	21.5	0.4	29.2	29.3	25.1	80.3	81.5	63.1	16.4	75.6	13.5	26.1	51.9	42.9
DPR [36]	82.4	38.0	78.6	8.7	0.6	26.0	3.9	11.1	75.5	84.6	53.5	21.6	71.4	32.6	19.3	31.7	40.0
PyCDA [27]	75.5	30.9	83.3	20.8	0.7	32.7	27.3	33.5	84.7	85.0	64.1	25.4	85.0	45.2	21.2	32.0	46.7
BL	55.6	23.8	74.6	9.2	0.2	24.4	6.1	12.1	74.8	79.0	55.3	19.1	39.6	23.3	13.7	25.0	33.5
Ours-w/oQT	69.4	30.9	79.8	21.3	0.5	30.2	31.0	22.7	82.3	82.6	66.4	15.2	79.1	20.5	26.7	48.2	44.2
Ours-w/oPL	70.3	32.1	77.8	22.9	0.8	29.6	32.4	24.3	81.7	80.1	62.9	22.0	75.4	26.2	25.3	51.0	44.7
Ours-w/oTKB	78.6	39.2	80.4	19.5	0.6	27.8	29.1	21.5	80.8	82.0	64.5	24.7	83.5	29.6	24.1	46.3	45.8
Ours-w/oAA	81.3	41.5	79.2	21.8	0.7	28.3	27.6	20.1	81.7	80.9	62.7	25.3	82.1	34.5	23.6	47.3	46.2
Ours	81.7	43.8	80.1	22.3	0.5	29.4	28.6	21.2	83.4	82.3	63.1	26.2	83.7	34.9	26.3	48.4	47.2

4.3. Experiments on Benchmark Datasets

Extensive experiments on several non-medical benchmark datasets are also conducted to further illustrate the generalization performance of our model. For a fair comparison, we set the same experimental data configuration with all comparable state-of-the-arts [16, 23, 25, 37, 38]. To be specific, in the training phase, GTA [32] and SYNTHIA [33] are regarded as the source dataset, and the training subset of Cityscapes [13] is treated as the target dataset. We use the validation subset of Cityscapes [13] for evaluation. Table 3 and Table 4 respectively report the results of transferring from GTA and SYNTHIA to Cityscapes. From Table 3 and Table 4, we have the following observations: 1) Our model outperforms all the existing advanced transfer models [16, 23, 34, 37, 38] about 0.5% ~ 11.1%, since two complementary modules could alternatively explore where and how to highlight transferable knowledge to bridge the domain gap, as shown in Figure 7. 2) Ablation studies about different components illustrate they play an important role in highlighting transferable domain-invariant knowledge to improve the transfer performance. 3) Our model achieves

larger improvements for those hard-to-transfer classes with various appearances among different datasets (*e.g.*, sidewalk, wall, motorbike, rider, sky and terrain) by selectively neglecting untransferable knowledge. In addition, Figure 8 presents the iteratively generated pseudo labels on GTA → Cityscapes task, which narrows the distribution divergence.

5. Conclusion

In this paper, we develop a new unsupervised semantic transfer model including two complementary modules (\mathcal{T}_D and \mathcal{T}_F), which alternatively explores transferable domain-invariant knowledge between labeled source gastroscopie lesions dataset and unlabeled target enteroscopy diseases dataset. Specifically, \mathcal{T}_D explores where to translate transferable visual characterizations while preventing untransferable translation. \mathcal{T}_F highlights how to augment those semantic representations with high transferability scores, which in return promotes the translation performance of \mathcal{T}_D . Comprehensive theory analysis and experiments on the medical endoscopic dataset and several non-medical benchmark datasets validate the effectiveness of our model.

References

- [1] Alex Alemi, Ian Fischer, Josh Dillon, and Kevin Murphy. Deep variational information bottleneck. In *ICLR*, 2017. 2, 4
- [2] Hans E. Atlason, Askeel Love, Sigurur Sigursson, Vilundur Gudnason, and Lotta Maria Ellingsen. Unsupervised brain lesion segmentation from mri using a convolutional auto-encoder. In *Medical Imaging: Image Processing*, 2018. 2
- [3] Caroline Baillard, Pierre Hellier, and Christian Barillot. Segmentation of brain 3d mr images using level sets and dense registration. *Medical Image Analysis*, Oct 2001. 2
- [4] Christoph Baur, Benedikt Wiestler, Shadi Albarqouni, and Nassir Navab. Fusing unsupervised and supervised deep learning for white matter lesion segmentation. In *Proceedings of The 2nd International Conference on Medical Imaging with Deep Learning*, volume 102, pages 63–72, Jul 2019. 2
- [5] Shai Ben-David, John Blitzer, Koby Crammer, Alex Kulesza, Fernando Pereira, and Jennifer Wortman Vaughan. A theory of learning from different domains. *Machine Learning*, 79:151–175, May 2010. 6
- [6] Christopher Bowles, Chen Qin, Ricardo Guerrero, Roger Gunn, Alexander Hammers, David Alexander Dickie, Maria Valds Hernandez, Joanna Wardlaw, and Daniel Rueckert. Brain lesion segmentation through image synthesis and outlier detection. *Neuroimage Clinical*, (16):643–658, Sept. 2017. 2
- [7] B. Bozorgtabar, S. Sedai, P. Kanti Roy, and R. Garnavi. Skin lesion segmentation using deep convolution networks guided by local unsupervised learning. *IBM J. Res. Dev.*, 61:6:1–6:8, July 2017. 2
- [8] Cheng Chen, Qi Dou, Hao Chen, Jing Qin, and Pheng-Ann Heng. Synergistic image and feature adaptation: Towards cross-modality domain adaptation for medical image segmentation. In *AAAI*, 2019. 1, 2
- [9] Liang-Chieh Chen, Yukun Zhu, George Papandreou, Florian Schroff, and Hartwig Adam. Encoder-decoder with atrous separable convolution for semantic image segmentation. In *The European Conference on Computer Vision (ECCV)*, September 2018. 5, 6, 7
- [10] Xiaoran Chen and Ender Konukoglu. Unsupervised detection of lesions in brain MRI using constrained adversarial auto-encoders. *arXiv preprint arXiv:1806.04972*, 2018. 2
- [11] Yi-Hsin Chen, Wei-Yu Chen, Yu-Ting Chen, Bo-Cheng Tsai, Yu-Chiang Frank Wang, and Min Sun. No more discrimination: Cross city adaptation of road scene segmenters. In *The IEEE International Conference on Computer Vision (ICCV)*, Oct 2017. 2
- [12] Jie-Zhi Cheng, Yi-Hong Chou, Chiun-Sheng Huang, Yeun-Chung Chang, Chui-Mei Tiu, Kuei-Wu Chen, and Chung-Ming Chen. Computer-aided US Diagnosis of Breast Lesions by Using Cell-based Contour Grouping. *Radiology*, 255(3):746–754, June 2010. 2
- [13] Marius Cordts, Mohamed Omran, Sebastian Ramos, Timo Rehfeld, Markus Enzweiler, Rodrigo Benenson, Uwe Franke, Stefan Roth, and Bernt Schiele. The cityscapes dataset for semantic urban scene understanding. In *The IEEE Conference on Computer Vision and Pattern Recognition (CVPR)*, June 2016. 6, 8
- [14] Zhengming Ding, Sheng Li, Ming Shao, and Yun Fu. Graph adaptive knowledge transfer for unsupervised domain adaptation. In *Proceedings of the European Conference on Computer Vision (ECCV)*, pages 37–52, 2018. 2
- [15] Zhengming Ding, Ming Shao, and Yun Fu. Robust multi-view representation: A unified perspective from multi-view learning to domain adaptation. In *IJCAI*, pages 5434–5440, 2018. 2
- [16] Jiahua Dong, Yang Cong, Gan Sun, and Dongdong Hou. Semantic-transferable weakly-supervised endoscopic lesions segmentation. In *The IEEE International Conference on Computer Vision (ICCV)*, October 2019. 1, 2, 6, 7, 8
- [17] Qi Dou, Cheng Ouyang, Cheng Chen, Hao Chen, and Pheng-Ann Heng. Unsupervised cross-modality domain adaptation of convnets for biomedical image segmentations with adversarial loss. In *Proceedings of the 27th International Joint Conference on Artificial Intelligence*, pages 691–697, 2018. 1, 2
- [18] Rui Gong, Wen Li, Yuhua Chen, and Luc Van Gool. Dlow: Domain flow for adaptation and generalization. In *The IEEE Conference on Computer Vision and Pattern Recognition (CVPR)*, June 2019. 2
- [19] Ian J. Goodfellow, Jean Pouget-Abadie, Mehdi Mirza, Bing Xu, David Warde-Farley, Sherjil Ozair, Aaron Courville, and Yoshua Bengio. Generative adversarial nets. In *Proceedings of the 27th International Conference on Neural Information Processing Systems - Volume 2*, pages 2672–2680, 2014. 2
- [20] Kaiming He, Xiangyu Zhang, Shaoqing Ren, and Jian Sun. Deep residual learning for image recognition. In *The IEEE Conference on Computer Vision and Pattern Recognition (CVPR)*, June 2016. 5, 7
- [21] Judy Hoffman, Eric Tzeng, Taesung Park, Jun-Yan Zhu, Phillip Isola, Kate Saenko, Alexei Efros, and Trevor Darrell. CyCADA: Cycle-consistent adversarial domain adaptation. In *Proceedings of the 35th International Conference on Machine Learning*, volume 80, pages 1989–1998, Jul 2018. 3
- [22] Judy Hoffman, Dequan Wang, Fisher Yu, and Trevor Darrell. Fcns in the wild: Pixel-level adversarial and constraint-based adaptation. *arXiv preprint arXiv:1612.02649*, 2016. 2
- [23] Weixiang Hong, Zhenzhen Wang, Ming Yang, and Junsong Yuan. Conditional generative adversarial network for structured domain adaptation. In *The IEEE Conference on Computer Vision and Pattern Recognition (CVPR)*, June 2018. 1, 2, 6, 8
- [24] Karla Horsch, Maryellen L. Giger, Luz A. Venta, and Carl J. Vyborny. Automatic segmentation of breast lesions on ultrasound. *Medical Physics*, 28(8):1652–1659, Aug. 2001. 2
- [25] Chen-Yu Lee, Tanmay Batra, Mohammad Haris Baig, and Daniel Ulbricht. Sliced wasserstein discrepancy for unsupervised domain adaptation. In *The IEEE Conference on Computer Vision and Pattern Recognition (CVPR)*, June 2019. 1, 2, 8
- [26] Yunsheng Li, Lu Yuan, and Nuno Vasconcelos. Bidirectional learning for domain adaptation of semantic segmentation. In *The IEEE Conference on Computer Vision and Pattern Recognition (CVPR)*, June 2019. 1, 2, 6, 7, 8

- [27] Qing Lian, Fengmao Lv, Lixin Duan, and Boqing Gong. Constructing self-motivated pyramid curriculums for cross-domain semantic segmentation: A non-adversarial approach. In *The IEEE International Conference on Computer Vision (ICCV)*, October 2019. 1, 2, 6, 7, 8
- [28] Yawei Luo, Ping Liu, Tao Guan, Junqing Yu, and Yi Yang. Significance-aware information bottleneck for domain adaptive semantic segmentation. In *The IEEE International Conference on Computer Vision (ICCV)*, October 2019. 2
- [29] Yawei Luo, Liang Zheng, Tao Guan, Junqing Yu, and Yi Yang. Taking a closer look at domain shift: Category-level adversaries for semantics consistent domain adaptation. In *The IEEE Conference on Computer Vision and Pattern Recognition (CVPR)*, June 2019. 1, 2, 6, 8
- [30] Can Qin, Haoxuan You, Lichen Wang, C.-C. Jay Kuo, and Yun Fu. Pointdan: A multi-scale 3d domain adaption network for point cloud representation. In *Advances in Neural Information Processing Systems 32*, pages 7190–7201. Curran Associates, Inc., 2019. 2
- [31] Dezs Ribli, Anna Horvth, Zsuzsa Unger, Pter Pollner, and Istvn Csabai. Detecting and classifying lesions in mammograms with Deep Learning. *Scientific Reports*, Mar 2018. 2
- [32] Stephan R. Richter, Vibhav Vineet, Stefan Roth, and Vladlen Koltun. Playing for data: Ground truth from computer games. In *The IEEE International Conference on Computer Vision (ICCV)*, 2016. 6, 8
- [33] German Ros, Laura Sellart, Joanna Materzynska, David Vazquez, and Antonio M. Lopez. The synthia dataset: A large collection of synthetic images for semantic segmentation of urban scenes. In *The IEEE Conference on Computer Vision and Pattern Recognition (CVPR)*, June 2016. 6, 8
- [34] Kuniaki Saito, Kohei Watanabe, Yoshitaka Ushiku, and Tatsuya Harada. Maximum classifier discrepancy for unsupervised domain adaptation. In *The IEEE Conference on Computer Vision and Pattern Recognition (CVPR)*, June 2018. 2, 8
- [35] Swami Sankaranarayanan, Yogesh Balaji, Arpit Jain, Ser Nam Lim, and Rama Chellappa. Learning from synthetic data: Addressing domain shift for semantic segmentation. In *The IEEE Conference on Computer Vision and Pattern Recognition (CVPR)*, June 2018. 2, 8
- [36] Yi-Hsuan Tsai, Kihyuk Sohn, Samuel Schulter, and Manmohan Chandraker. Domain adaptation for structured output via discriminative patch representations. In *The IEEE International Conference on Computer Vision (ICCV)*, October 2019. 1, 2, 6, 7, 8
- [37] Yi-Hsuan Tsai, Wei-Chih Hung, Samuel Schulter, Kihyuk Sohn, Ming-Hsuan Yang, and Manmohan Chandraker. Learning to adapt structured output space for semantic segmentation. In *The IEEE Conference on Computer Vision and Pattern Recognition (CVPR)*, June 2018. 1, 2, 6, 8
- [38] Tuan-Hung Vu, Himalaya Jain, Maxime Bucher, Matthieu Cord, and Patrick Perez. Advent: Adversarial entropy minimization for domain adaptation in semantic segmentation. In *The IEEE Conference on Computer Vision and Pattern Recognition (CVPR)*, June 2019. 2, 6, 7, 8
- [39] Qiang Wang, Huijie Fan, Gan Sun, Yang Cong, and Yandong Tang. Laplacian pyramid adversarial network for face completion. *Pattern Recognition*, 88:493–505, 2019. 2
- [40] Qiang Wang, Huijie Fan, Gan Sun, Weihong Ren, and Yandong Tang. Recurrent generative adversarial network for face completion. *IEEE Transactions on Multimedia*, 2020. 2
- [41] Zuxuan Wu, Xintong Han, Yen-Liang Lin, Mustafa Gokhan Uzunbas, Tom Goldstein, Ser Nam Lim, and Larry S. Davis. Dcan: Dual channel-wise alignment networks for unsupervised scene adaptation. In *The European Conference on Computer Vision (ECCV)*, September 2018. 2, 8
- [42] Yan Xu, Zhipeng Jia, Liang-Bo Wang, Yuqing Ai, Fang Zhang, Maode Lai, and Eric I-Chao Chang. Large Scale Tissue Histopathology Image Classification, Segmentation and Visualization via Deep Convolutional Activation Features. *BMC Bioinformatics*, 2017. 2
- [43] Yang Zhang, Philip David, and Boqing Gong. Curriculum domain adaptation for semantic segmentation of urban scenes. In *The IEEE International Conference on Computer Vision (ICCV)*, Oct 2017. 2
- [44] Jun-Yan Zhu, Taesung Park, Phillip Isola, and Alexei A. Efros. Unpaired image-to-image translation using cycle-consistent adversarial networks. *arXiv preprint arXiv:1703.10593*, 2017. 5, 6
- [45] Yang Zou, Zhiding Yu, B.V.K. Vijaya Kumar, and Jinsong Wang. Unsupervised domain adaptation for semantic segmentation via class-balanced self-training. In *The European Conference on Computer Vision (ECCV)*, September 2018. 2, 8